Natural ZMP Trajectories for Biped Robot Reference Generation

Kemalettin Erbatur, *Member, IEEE*, and Okan Kurt

Abstract—The control of a biped humanoid is a challenging task due to the hard-to-stabilize dynamics. Walking reference trajectory generation is a key problem. Linear Inverted Pendulum Model (LIPM) and Zero Moment Point (ZMP) Criterion-based approaches in stable walking reference generation are reported. In these methods, generally, the ZMP reference during a stepping motion is kept fixed in the middle of the supporting foot sole. This kind of reference generation lacks naturalness, in that the ZMP in the human walk does not stay fixed, but it moves forward under the supporting foot. This paper proposes a reference generation algorithm based on the LIPM and moving support foot ZMP references. The application of Fourier series approximation simplifies the solution, and it generates a smooth ZMP reference. A simple inverse kinematics-based joint space controller is used for the tests of the developed reference trajectory through full-dynamics 3-D simulation. A 12-DOF biped robot model is used in the simulations. Simulation studies suggest that the moving ZMP references are more energy efficient than the ones with fixed ZMP under the supporting foot. The results are promising for implementations.

Index Terms—Humanoid robot walking reference generation, legged locomotion, Zero Moment Point (ZMP).

I. INTRODUCTION

HUMANOID robotics have attracted the attention of many researchers in the past 35 years. It is currently one of the most exciting topics in the field of robotics, and there are many projects on this topic [1]–[7]. The motivation of the research is the suitability of the biped structure for tasks in the human environment, and the goal of the studies in this area is to reach the human walking dexterity, efficiency, stability, effectiveness, and flexibility.

The control of a biped humanoid is a challenging task due to the many degrees of freedom involved and the nonlinear and hard-to-stabilize dynamics [8], [9]. Walking reference trajectory generation is a key problem. Methods ranging from trial and error to the use of optimization techniques with energy, or control effort minimization constraints are applied as solutions. A very intuitive criterion used for the reference generation is that the reference trajectory should be suitable to be followed by the robot with its natural dynamics, without the use of extensive control intervention. Reference generation

techniques with the Linear Inverted Pendulum Model (LIPM) are based on this idea [10]–[12]. Simply stated, the walking cycle is achieved by letting the robot start falling into the walking direction and to switch supporting legs to avoid the complete falling of the robot.

Yet, another intuitive demand for the biped robot reference generation is that the reference trajectory should be a stable one, in the sense that it should not lead to unrecoverable falling motion. The Zero Moment Point (ZMP) Criterion [8] introduced to the robotics literature in early 1970s is widely employed in the stability analysis of biped robot walk. Improved versions of the LIPM-based reference generation, obtained by applying the ZMP criterion in the design process, are reported too [13]–[16]. The ZMP criterion can be applied to generate reference trajectories for more complicated motion scenarios too [17]–[20]. In creating walking trajectories, the ZMP during a stepping motion is kept fixed in the middle of the supporting foot sole for the stability, while the robot center of mass (CoM) follows the Linear Inverted Pendulum path.

Although reference generation with the LIPM and fixed ZMP reference positions is successfully employed, this kind of reference generation lacks naturalness at one point. Investigations revealed that the ZMP in the human walk does not stay fixed under the supporting foot. Rather, it moves forward from the heel to the toe direction [21]–[24]. It should, however, be noted that the discussion of naturalness of a gait is not an easy one. The forward moving ZMP constitutes a part in naturalness, but it does not necessarily create a fully natural looking walk. The definition of a natural walk is sought not only for legged robot locomotion, but also in the field of human perception research. The work reported in [25] indicates that perceived naturalness of a gait can be influenced by the motion of any limb segment, and primarily determined by the movements of the lower leg. The relationship between the motion phase analysis and a subjective description of gait, such as a normal gait versus a tired gait is investigated in [26]. The fact that humans walk in an energy efficient manner [27] can be used as a measure of naturalness of a robot walk too.

Reference [23] proposes the idea of using variable ZMP to generate a dynamically stable gait in terms of linear inverted pendulum approach. They consider it to follow first-order functions from the heel to toe of the supporting foot in single support phase.

This paper takes an approach similar to [24] and proposes a reference generation technique based on the LIPM and moving support foot ZMP references. As in [28], the application of Fourier series approximation to the solutions of the Linear Inverted Pendulum dynamics equations simplifies the procedure.

K. Erbatur is with the Faculty of Engineering and Natural Sciences, Sabanci University, 34956 Istanbul, Turkey (e-mail: erbatur@sabanciuniv.edu).

O. Kurt was with Sabanci University, 34956 Istanbul, Turkey. He is now with the Product Development Department, Ford Otosan A.Ş., 41470 Kocaeli, Turkey (e-mail: okurt5@ford.com).
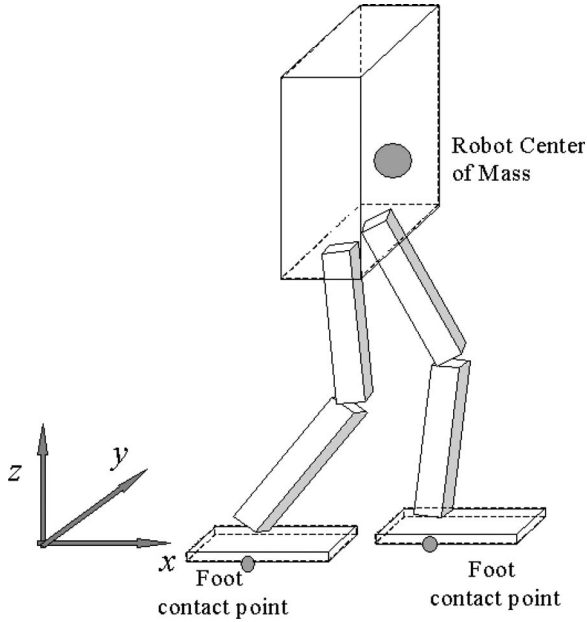
Fig. 1.   Typical kinematic arrangement of a biped robot. It resembles an inverted pendulum in single support phases.

ZMP reference for the double support phase is generated by smoothing techniques. Robot CoM reference is obtained from the desired ZMP trajectory. The computation of smooth swing foot trajectories completes the reference generation for locomotion. A simple inverse kinematics-based independent joint position controller is employed, and the reference generation techniques are tested in a 3-D full dynamics simulation and animation environment with a 12-DOF biped robot model. For comparison purposes, simulations are carried out with fixed single support ZMP reference trajectories too.

The reference generation with natural moving ZMP trajectories and the control of locomotion are discussed in Sections II and III, respectively. Section IV presents the simulation results and their analysis. Finally, in Section V we conclude with some remarks.

II. REFERENCE GENERATION WITH NATURAL ZMP TRAJECTORIES

This section first introduces the LIPM and derives a relationship between the ZMP and the location of the robot CoM. Discussion of suitable ZMP references and methods for obtaining CoM reference trajectories from given ZMP references follow.

A. LIMP and ZMP

The discussion is independent from the kinematic arrangement of the legged robot. The LIPM derivations are even independent from the number of the legs.

The only assumption is that the mass of the legs should be much less than the robot mass. In fact, the method is still applicable with heavy legs, but with a degradation of relative stability of the walk. Although there is no limitation on the kinematic arrangement for the ZMP and CoM reference generation discussions, there is a limitation for the control structure described in this paper. This is, the legs should have
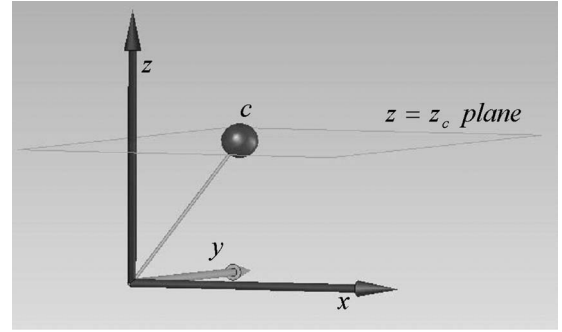

Fig. 2.   Linear inverted pendulum.

at least 6 DOF. The sketch in Fig. 1 shows an example of a robot structure for which the reference generation and control algorithms presented below can be applied: A biped robot with 6-DOF legs.

The full dynamics description for a robot structure like the one shown in Fig. 1 is highly nonlinear multiple degree of freedom and coupled. Its motion equation can be expressed as

$$\begin{bmatrix} H_{11} & H_{12} & H_{13} \\ H_{21} & H_{22} & H_{23} \\ H_{31} & H_{32} & H_{33} \end{bmatrix} \begin{pmatrix} \dot{v}_\mathrm{B} \\ \dot{\omega}_\mathrm{B} \\ \ddot{\theta} \end{pmatrix} + \begin{pmatrix} c_1 \\ c_2 \\ c_3 \end{pmatrix} + \begin{pmatrix} u_{\mathrm{E}_1} \\ u_{\mathrm{E}_2} \\ u_{\mathrm{E}_3} \end{pmatrix} = \begin{pmatrix} 0 \\ 0 \\ \tau \end{pmatrix} \tag{1}$$

where H_{ij} for $(i,j) \in \{1,2,3\}$ are submatrices of the robot inertia matrix. v_B is the linear velocity of the robot body coordinate frame center with respect to a fixed world coordinate frame, ω_B is the angular velocity of the robot body coordinate frame with respect to a fixed world coordinate frame, and θ is the vector of joint displacements of the biped. The vector formed by augmenting c_1, c_2, and c_3 is termed as the bias vector in this dynamics equation. u_{E_1} is the net force effect, and u_{E_2} is the net torque effect of the reaction forces on the robot body. u_{E_3} stands for the effect of reaction forces on the robot joints. Reactive forces are generated by environmental interaction. τ is the generalized joint control vector, typically consisting of joint actuation torques for a robot with revolute joints. H_{11}, H_{12}, H_{21}, and H_{22} are 3×3 matrices. For a 12-DOF robot with 6 DOF at each leg, as described in the previous section, H_{13} is 3×12, H_{23} is 3×12, H_{31} is 12×3, H_{32} is 12×3, and H_{33} is 12×12 [29]. The closed form solutions of the matrices in this expression are very difficult to obtain. Rather, Newton–Euler recursive formulations are used in their computation [30], [31].

Although obtaining such a model is very useful for the simulation and test of reference generation and control methods, the structure in (1) is too complex to serve as an intuitive model which can help in developing guidelines and basics for the walking control. Simpler models are more suitable for controller synthesis. The inverted pendulum model is such a simple model. The body (trunk) is approximated by a point mass concentrated at the CoM of the robot. This point mass is linked to a stable (not sliding) contact point on the ground via a massless rod, which is the idealized model of a supporting leg. The swing leg is assumed to be massless too. Fig. 2 shows an inverted pendulum. In this figure, $c = \begin{pmatrix} c_x & c_y & c_z \end{pmatrix}^\mathrm{T}$ stands for the coordinates of this point mass. Although much simpler

than (1), the equations of motion of the inverted pendulum model are still coupled and nonlinear. One more assumption, however, yields a linear system which is uncoupled in the x- and y-directions. This is the assumption of fixed height of the CoM. This model is called LIPM, and it is simple enough to work on and devise algorithms for reference generation [12]. The equations of motion of the CoM with the LIPM are as follows:

$$\ddot{c}_x = \frac{g}{z_c}x + \frac{1}{mz_c}u_p \qquad (2)$$

$$\ddot{c}_y = \frac{g}{z_c}y - \frac{1}{mz_c}u_r. \qquad (3)$$

In this equation, m is the mass of the body (point mass), z_c is the height of the plane on which the motion of the point mass is constrained, and g is the gravity constant (9.806 m/s^2). u_p and u_r are the pitch (about y-axis) and roll (about x-axis) control torques, respectively. These act at the support point (origin in Fig. 2) of the linear inverted pendulum.

The idea that the energy efficient references should allow the robot to move in compliance with the natural fall due to the gravity (without too large control effort by the joint actuators) can be employed with this model. References consisting of freely falling (tilting aside) segments are developed in [12] with the LIPM.

Since the solutions of (2) and (3) in the unactuated case $(u_p = u_r = 0)$ are unbounded functions, and therefore, the computation of a reference trajectory from freely falling segments should carefully be carried out in order to obtain a stable reference. Stability of the walk is trivially the most wanted feature of a reference trajectory. In biped robotics, the most widely accepted criterion for stability is based on the location of the ZMP [8]. For the arrangement in Fig. 2, the ZMP is defined as the point on the $x-y$ plane about which no horizontal torque components exist.

The expressions for the ZMP coordinates p_x and p_y for the point mass structure in Fig. 2 are [28]

$$p_x = c_x - \frac{z_c}{g}\ddot{c}_x \qquad (4)$$

$$p_y = c_y - \frac{z_c}{g}\ddot{c}_y. \qquad (5)$$

The result in (4) can be obtained by a torque balance equation in the $x-z$ plane, as shown in Fig. 3.

In order to have zero net moment at the "pivot point" in Fig. 3, the torque due to gravity (Δxmg) should be balanced by the torque generated by the reaction force due to the acceleration of the point mass in the x-direction $(z_c m\ddot{x})$. This gives a solution for Δx and, hence, the touching point p_x for the zero moment condition. A similar discussion for the $y-z$ plane can yield (5).

B. Fixed and Moving ZMP References

Equations (4) and (5) are equations relating the ZMP and the CoM. For reference generation purposes, a suitable ZMP trajectory can be assigned without difficulty. The only constraint for stability of the robot is that the ZMP should always lie in
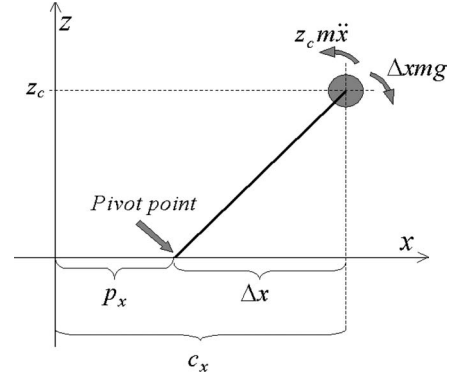

Fig. 3.   Diagram for torque balance in the $x-z$ plane.

the supporting polygon defined by the foot or feet touching the ground. The most intuitive choice for the ZMP location is the middle of the supporting foot sole. Choi *et al.* [28] created the reference ZMP trajectory shown in Fig. 4 with this idea. In this figure, A is the distance between the foot centers in the y-direction, B is the step size, and T is half of the walking period. As can be observed from Fig. 4, firstly, step locations are determined.

The selection of the step locations can be based on the size of the robot and the nature of the task performed by the robot. The staircaselike p_z and the square-wave structured p_y curves are fully defined by the selection of support foot locations if the half period T is given too. Similar to the step size, the step period can also be determined by the physical size and properties of the robot and by the application.

However, the naturalness of the walk is not addressed in [28]. As previously mentioned, the starting point of the reference ZMP curves in that work is the choice that ZMP stays at a fixed point under the sole, although investigations [21], [22] of the human ZMP revealed that it moves forward under the sole (Fig. 5). Furthermore, the curves in Fig. 4 imply that the transition from left single support phase to the right support phase is instantaneous, without a double support phase.

The p_x reference curve shown in Fig. 6(b) is employed in this paper. It can be noted that this figure illustrates a moving ZMP. As previously mentioned, a complete definition of naturalness of walk is difficult to obtain, and the curve in this figure is not necessarily the most natural ZMP reference. However, it is more natural than a fixed ZMP curve because it is more similar to the human ZMP. The parameter b in the figure defines the range of the ZMP motion under the sole. A symmetric trajectory centered at the foot center is assumed here. Although b can be interpreted as the half of the foot length, this interpretation is not a must: ZMP may move on the line connecting the heel with the toes without covering this line completely too.

Smooth transition between single support phases with a double support phase is achieved by an additional smoothing action discussed later in this section.

C. Computation of CoM References

Having defined the curves and, hence, the mathematical functions for $p_x^{ref}(t)$ and $p_y^{ref}(t)$, (4), (5), and Laplace transform

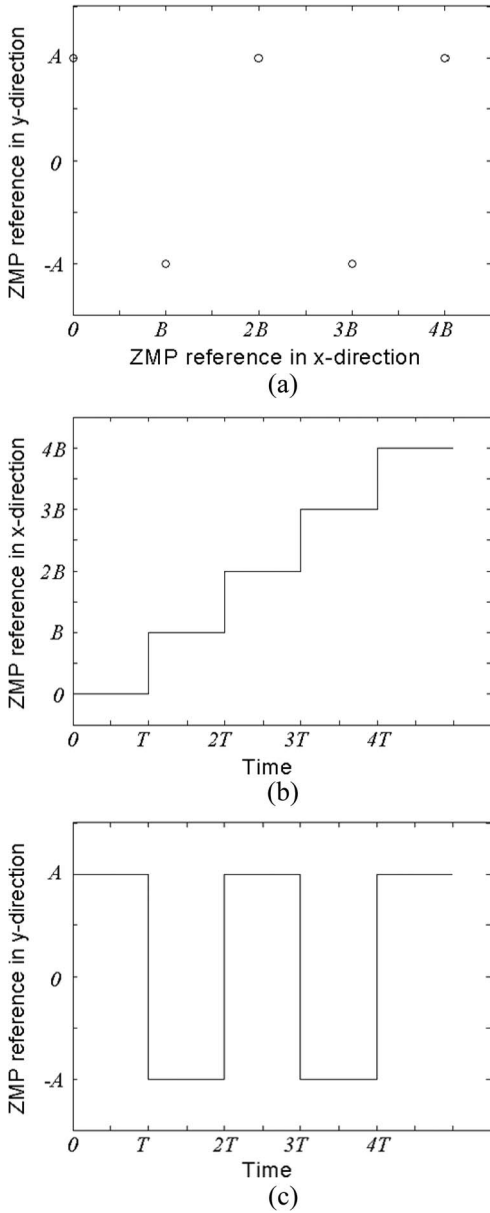Fig. 4. Fixed ZMP references. (a) $p_y^{\mathrm{ref}}-p_x^{\mathrm{ref}}$ relation on the $x-y$ plane. ZMP references and stepping positions overlap. (b) p_x^{ref}, the x-axis ZMP reference. (c) p_y^{ref}, the y-axis ZMP reference.
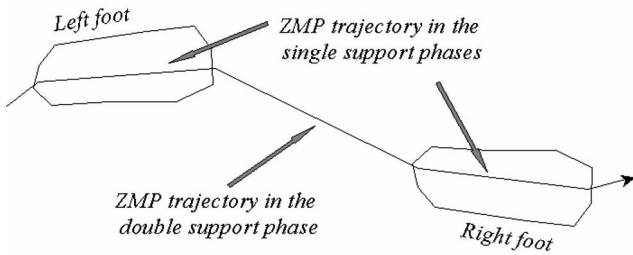

Fig. 5. Natural ZMP trajectory.

techniques can be employed to obtain the solution for the CoM position references $c_x^{\mathrm{ref}}(t)$ and $c_y^{\mathrm{ref}}(t)$ ($c_z^{\mathrm{ref}}(t) = z_{\mathrm{c}}$, which is a constant in the LIPM). After having found the required CoM reference trajectories, a position control scheme for the robot

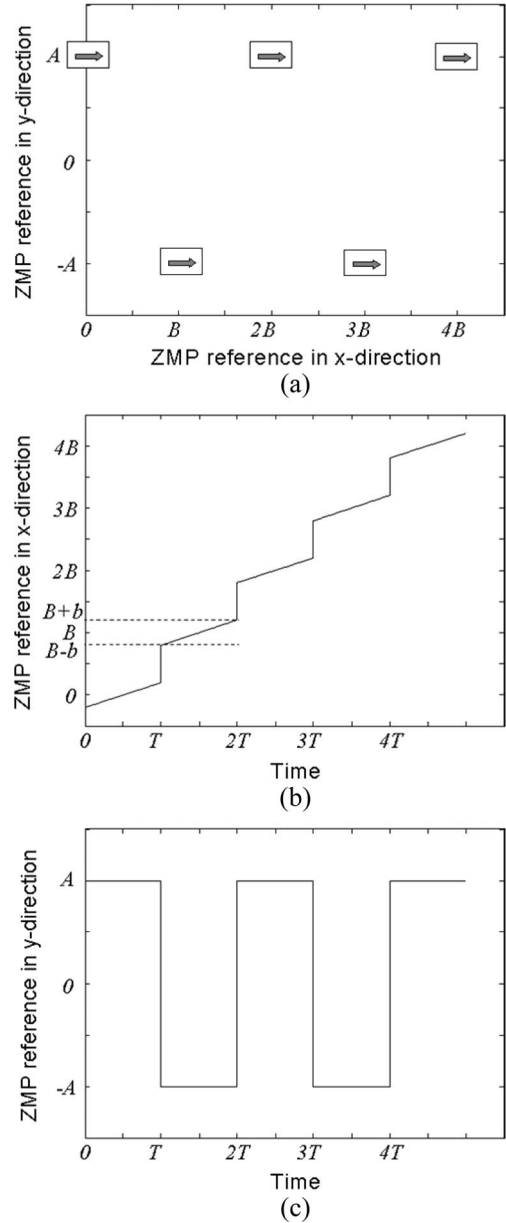Fig. 6. Moving ZMP reference. (a) $p_y^{\mathrm{ref}}-p_x^{\mathrm{ref}}$ relation on the $x-y$ plane. (b) p_x^{ref}, a natural x-axis ZMP reference. Note the difference of the x-reference with the one shown in Fig. 4. (c) p_y^{ref}, the y-axis ZMP reference.

joints with references obtained by inverse kinematics from these CoM locations can be obtained. Cartesian control techniques can be applied for achieving desired CoM positions too.

The mathematical descriptions of the $p_x^{\mathrm{ref}}(t)$ and $p_y^{\mathrm{ref}}(t)$ in Fig. 6 are given by

$$p_x^{\mathrm{ref}} = \frac{2b}{T}\left(t - \frac{T}{2}\right) + (B - 2b)\sum_{k=1}^{\infty} u(t - kT_0) \qquad (6)$$

$$p_y^{\mathrm{ref}} = Au(t) + 2A\sum_{k=1}^{\infty}(-1)^k u(t - kT_0) \qquad (7)$$

where $u(\cdot)$ represents the unit step function.

Defining $\omega_n \equiv \sqrt{g/z_c}$, we can rewrite (4) and (5) for the reference variables as follows:

$$\ddot{c}_x^{\mathrm{ref}} = \omega_n^2 c_x^{\mathrm{ref}} - \omega_n^2 p_x^{\mathrm{ref}} \tag{8}$$

$$\ddot{c}_y^{\mathrm{ref}} = \omega_n^2 c_y^{\mathrm{ref}} - \omega_n^2 p_y^{\mathrm{ref}}. \tag{9}$$

Applying the Laplace transform, we can obtain

$$C_x^{\mathrm{ref}}(s) = \frac{1}{1-(1/\omega_n^2)\,s^2}\left[P_x^{\mathrm{ref}}(s) - \frac{1}{\omega_n^2}c_x^{\mathrm{ref}}(0)s - \frac{1}{\omega_n^2}\dot{c}_x^{\mathrm{ref}}(0)\right] \tag{10}$$

$$C_y^{\mathrm{ref}}(s) = \frac{1}{1-(1/\omega_n^2)\,s^2}\left[P_y^{\mathrm{ref}}(s) - \frac{1}{\omega_n^2}c_y^{\mathrm{ref}}(0)s - \frac{1}{\omega_n^2}\dot{c}_y^{\mathrm{ref}}(0)\right]. \tag{11}$$

Equations (6) and (10) with zero initial conditions yield

$$C_x^{\mathrm{ref}}(s) = \frac{1}{1-(1/\omega_n^2)\,s^2}P_x^{\mathrm{ref}}(s)$$

$$= \frac{1}{1-(1/\omega_n^2)\,s^2}\left[\frac{2b}{T}\frac{1}{s^2} - b\frac{1}{s} + (B-2b)\frac{1}{s}\sum_{k=1}^{\infty}e^{-kTs}\right]$$

$$= \left[\frac{1}{s} - \frac{s}{s^2-\omega_n^2}\right]\left[\frac{2b}{T}\frac{1}{s} - b + (B-2b)\sum_{k=1}^{\infty}e^{-kTs}\right]$$

$$= \frac{2b}{T}\frac{1}{s^2} - b\frac{1}{s} + (B-2b)\frac{1}{s}\sum_{k=1}^{\infty}e^{-kTs} - \frac{2b}{T}\frac{1}{s^2-\omega_n^2}$$

$$+ b\frac{s}{s^2-\omega_n^2} - (B-2b)\frac{s}{s^2-\omega_n^2}\sum_{k=1}^{\infty}e^{-kTs}. \tag{12}$$

Therefore, the time domain solution for the x-direction reference for the CoM can be computed by inverse Laplace transform as

$$c_x^{\mathrm{ref}}(t) = \frac{2b}{T}t - b1(t) - \frac{2b}{T\omega_n}\sinh\omega_n t + b\cosh\omega_n t$$

$$+ (B-2b)\sum_{k=1}^{\infty}(1-\cosh\omega_n(t-kT))\,1(t-kT). \tag{13}$$

Similarly, from (7) and (11), with zero initial conditions the Laplace transform $C_y^{\mathrm{ref}}(s)$ can be computed as

$$C_y^{\mathrm{ref}}(s) = \frac{1}{1-(1/\omega_n^2)\,s^2}P_y^{\mathrm{ref}}(s)$$

$$= \frac{1}{1-(1/\omega_n^2)\,s^2}\left[A\frac{1}{s} + 2A\frac{1}{s}\sum_{k=1}^{\infty}(-1)^k e^{-kTs}\right]$$

$$= \left[\frac{1}{s} - \frac{s}{s^2-\omega_n^2}\right]\left[A + 2A\sum_{k=1}^{\infty}(-1)^k e^{-kTs}\right] \tag{14}$$

and inverse Laplace transformation results in the expression

$$c_y^{\mathrm{ref}} = 2A\sum_{k=1}^{\infty}(-1)^k\left(1-\cosh\omega_n(t-kT_0)\right)1(t-kT_0). \tag{15}$$

It can be noted that the solutions for c_x^{ref} and c_y^{ref} consist of cosh functions (which are unbounded) and further, the result is very sensitive to the value of $g/z_c(=\omega_n^2)$. Therefore, the application of these solutions is quite difficult. Reference [28] also indicates similar results for the reference ZMP trajectories in Fig. 4 and proposes an approximate solution with the use of Fourier series representation to overcome this difficulty and to obtain CoM references suitable for robust implementation of the reference generation.

Taking an approach similar to the one in [28], this paper develops an approximate solution for the c_x and c_y references corresponding to the moving ZMP references in Fig. 6. Note that the y-direction ZMP reference $p_y^{\mathrm{ref}}(t)$ is a periodic function with the period $2T$. It is reasonable to assume that $c_y^{\mathrm{ref}}(t)$ is a periodic function too and that it has the same period. Hence, it can be approximated by a Fourier series

$$c_y^{\mathrm{ref}}(t) = \frac{a_0}{2} + \sum_{k=1}^{\infty}a_k\cos\left(\frac{2\pi k t}{2T}\right) + b_k\sin\left(\frac{2\pi k t}{2T}\right). \tag{16}$$

By (9) and (16), p_y^{ref} can be expressed as

$$p_y^{\mathrm{ref}}(t) = c_y^{\mathrm{ref}} - \frac{z_c}{g}\ddot{c}_y^{\mathrm{ref}}$$

$$= \frac{a_0}{2} + \sum_{k=1}^{\infty}a_k\left(1+\frac{\pi^2 k^2}{\omega_n^2 T^2}\right)\cos\left(\frac{2\pi k t}{2T}\right)$$

$$+ b_k\left(1+\frac{\pi^2 k^2}{\omega_n^2 T^2}\right)\sin\left(\frac{2\pi k t}{2T}\right). \tag{17}$$

Noting that this expression in the form of a Fourier series for $p_y^{\mathrm{ref}}(t)$, and since $p_y^{\mathrm{ref}}(t)$ is an odd function, we can conclude that the coefficients $a_0/2$ and $a_k(1+(\pi^2 k^2)/(\omega_n^2 T^2))$ for $k = 1,2,3,\ldots$ are zero. In order to compute the coefficients $b_k(1+(\pi^2 k^2)/(\omega_n^2 T^2))$, we can employ the Fourier integral

$$b_k\left(1+\frac{\pi^2 k^2}{\omega_n^2 T^2}\right) = \frac{2}{2T}\int_0^{2T}p_y^{\mathrm{ref}}\sin\left(\frac{2\pi k t}{2T}\right)dt. \tag{18}$$

As a result, the Fourier coefficients of $c_y^{\mathrm{ref}}(t)$ in (16) can be obtained as

$$a_0 = 0$$

$$a_k = 0$$

$$b_k = \frac{2AT^2\omega_n^2(1-\cos k\pi)}{k\pi\,(T^2\omega_n^2 + k^2\pi^2)}, \qquad k = 1,2,3,\ldots. \tag{19}$$

The second step is finding the Fourier series coefficients for c_x^{ref}. $p_x^{\mathrm{ref}}(t)$ in Fig. 6 is not a periodic function. It cannot be expressed as a Fourier series. However, it can be noted that this function is composed of a periodic function $p_x'^{\mathrm{ref}}$ defined by

$$p_x'^{\mathrm{ref}} = -\frac{(B-2b)}{T}\left(t-\frac{T}{2}\right) \qquad \text{for } t \in [0,T]$$

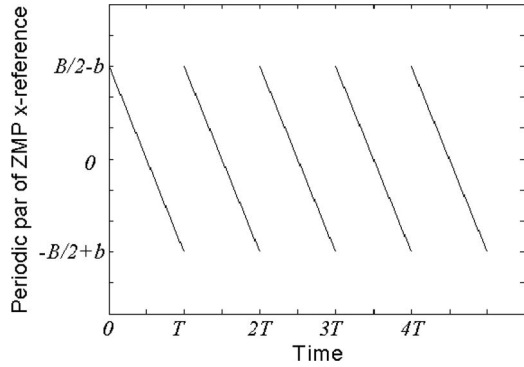$$p_x'^{\mathrm{ref}}(t+T) = p_x'^{\mathrm{ref}}(t) \tag{20}$$

Fig. 7. $p_x'^{\text{ref}}(t)$, the periodic part of the x-direction ZMP reference $p_x^{\text{ref}}(t)$.

and a nonperiodic one $((B/T)(t - (T/2)))$. The periodic and nonperiodic parts of $p_x^{\text{ref}}(t)$ are shown in Fig. 7. It is again a reasonable assumption that c_x^{ref} has a periodic part and a nonperiodic part too. Furthermore, if we suppose that the two nonperiodic parts (of $p_x^{\text{ref}}(t)$ and c_x^{ref}) are nonequal, then the difference $p_x^{\text{ref}}(t) - c_x^{\text{ref}}$ will be nonperiodic. This is not expected in a continuous walk as the one shown in Fig. 6.

Therefore, we conclude that the nonperiodic parts of the two functions are equal. Note that, as shown in Fig. 7, the period of the periodic part of $p_x^{\text{ref}}(t)$ is T, and we can make the same statement for the period of the periodic part of c_x^{ref}. Finally, c_x^{ref} can be expressed as

$$c_x^{\text{ref}} = \frac{B}{T}\left(t - \frac{T}{2}\right) + \frac{\alpha_0}{2} + \sum_{n=1}^{\infty} \alpha_n \cos\left(\frac{2\pi n t}{T}\right) + \beta_n \sin\left(\frac{2\pi n t}{T}\right). \tag{21}$$

Recalling (4), with (21), the expression for $p_x^{\text{ref}}(t)$ with a Fourier series is

$$\begin{aligned} p_x^{\text{ref}}(t) &= c_x^{\text{ref}} - \frac{z_c}{g}\ddot{c}_x^{\text{ref}} \\ &= \frac{B}{T}\left(t - \frac{T}{2}\right) + \frac{\alpha_0}{2} + \sum_{n=1}^{\infty} \alpha_k \left(1 + \frac{\pi^2 k^2}{\omega_n^2 T^2}\right) \\ &\quad \times \cos\left(\frac{2\pi k t}{T}\right) + \beta_k \left(1 + \frac{\pi^2 k^2}{\omega_n^2 T^2}\right) \sin\left(\frac{2\pi k t}{T}\right). \end{aligned} \tag{22}$$

Therefore, the Fourier coefficients of $p_x'^{\text{ref}}(t)$, the periodic part of $p_x^{\text{ref}}(t)$, are $\alpha_0/2$, $\alpha_k(1 + \pi^2 k^2/\omega_n^2 T^2)$, and $\beta_k(1 + \pi^2 k^2/\omega_n^2 T^2)$ for $k = 1, 2, 3, \ldots$ The Fourier coefficients $\alpha_0/2$, $\alpha_k(1 + \pi^2 k^2/\omega_n^2 T^2)$ of $p_x'^{\text{ref}}(t)$ shown in Fig. 7 are zero because this is an odd function. The coefficients for $\beta_k(1 + (\pi^2 k^2)/(\omega_n^2 T^2))$ can be found by

$$\beta_k \left(1 + \pi^2 k^2/\omega_n^2 T^2\right) = \frac{2}{T}\int_0^T p_x'^{\text{ref}}(t) \sin\left(\frac{2\pi k t}{T}\right) dt. \tag{23}$$

This yields the result

$$\begin{aligned} \alpha_0/2 &= 0 \\ \alpha_k &= 0 \\ \beta_k &= \frac{(B - 2b)T^2 \omega_n^2}{k\pi\left(T^2\omega_n^2 + k^2\pi^2\right)} \qquad \text{for } k = 1, 2, 3, \ldots. \end{aligned} \tag{24}$$
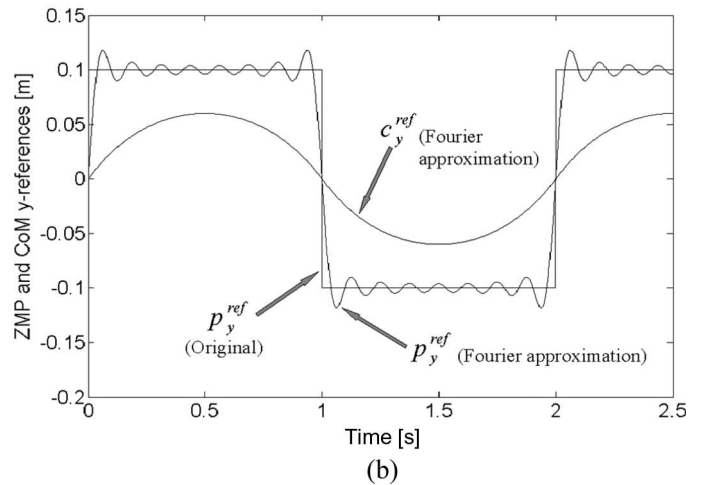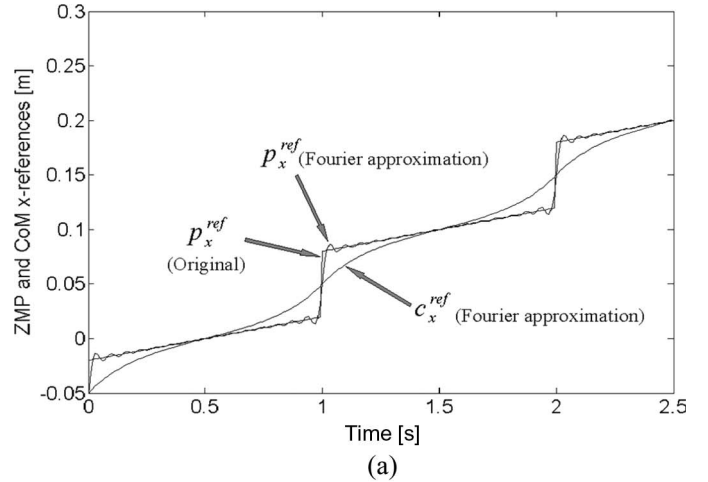

(a)

(b)

Fig. 8. CoM reference curves together with the corresponding original and Fourier approximation ZMP reference curves. (a) c_x^{ref} and (b) $c_y^{\text{ref}}(t)$.

and c_x^{ref} can then be written as

$$c_x^{\text{ref}} = \frac{B}{T}\left(t - \frac{T}{2}\right) + \sum_{k=1}^{\infty} \frac{(B - 2b)T^2 \omega_n^2}{k\pi\left(T^2\omega_n^2 + k^2\pi^2\right)} \sin\left(\frac{2\pi k t}{T}\right). \tag{25}$$

The curves obtained for c_x^{ref} and $c_y^{\text{ref}}(t)$ are shown in Fig. 8 together with the corresponding original (as defined in Fig. 6) and Fourier approximation ZMP reference curves. In Fig. 8, the following parameter values are used: $A = 0.1$, $B = 0.1$, $b = 0.02$, $T = 1$. The infinite sums in (16), (17), (21), and (22) are approximated by finite sums of N terms ($N = 15$). These parameter values are valid for the rest of the figures in this section too.

Fig. 9 shows the fixed ZMP [28] and moving ZMP CoM reference curves in the x-direction. It can be seen that the moving ZMP results in a x-direction CoM reference which closer to a straight line. This suggests that the energy consumption for locomotion is less with the moving ZMP than that with the fixed ZMP. This is expected from a natural reference trajectory, and this result is in parallel with the results in [23]. Section IV quantifies the difference in the energy consumption via simulation studies.
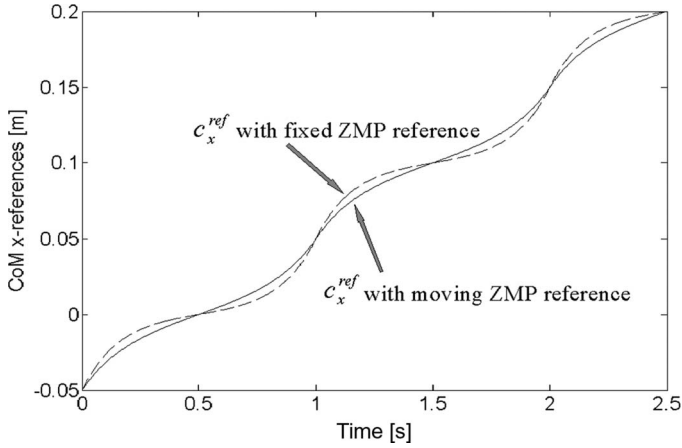
Fig. 9. Comparison of the fixed ZMP and moving ZMP CoM x-direction references. The CoM reference corresponding to the moving ZMP reference oscillates with smaller amplitude.
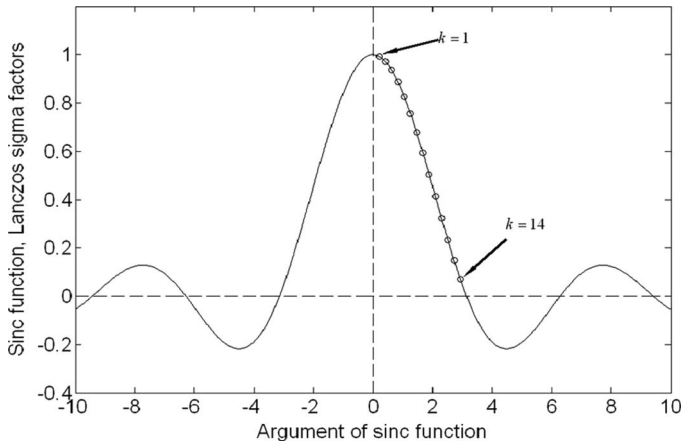

Fig. 10. Lanczos sigma factor values on the sinc function.

D. Reference Smoothing

The ZMP reference moving forward under the sole is introduced by the discussion above. However, still missing is the double support phase. The introduction of the double support phase is achieved by a smoothing function in this paper. The Lanczos sigma factors [32] are employed as a method to solve the Gibbs phenomenon [33], i.e., nonuniform convergence of the Fourier series (here evident from the peaks shown in Fig. 8 at the discontinuities of the approximated function). In this paper, however, the application of the Lanczos sigma factors has the second role of smoothing the abrupt changes in the reference ZMP functions and creating double support phases.

The Lanczos Sigma Factor is defined as the function

$$\text{sinc}(k\pi/N) = \frac{\sin(k\pi/N)}{k\pi/N} \quad (26)$$

where N is one more that the number of terms in a Fourier series approximation. When applied on a Fourier series, the series after the Lanczos Sigma smoothing can be written as

$$f(\theta) = \frac{\phi_0}{2} + \sum_{k=1}^{N-1} \text{sinc}\left(\frac{k\pi}{N}\right)[\phi_k \cos(k\theta) + \psi_k \sin(k\theta)]. \quad (27)$$
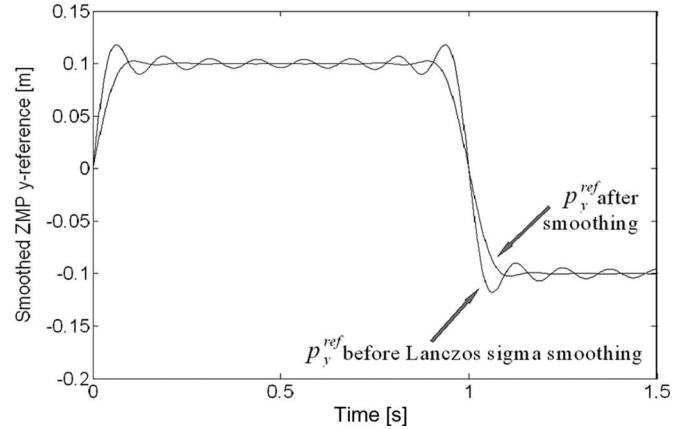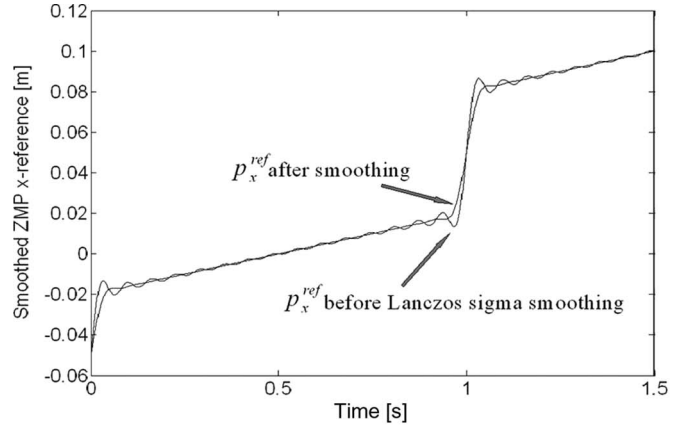

Fig. 11. Effect of Lanczos sigma smoothing on the x- and y-direction (ZMP references).
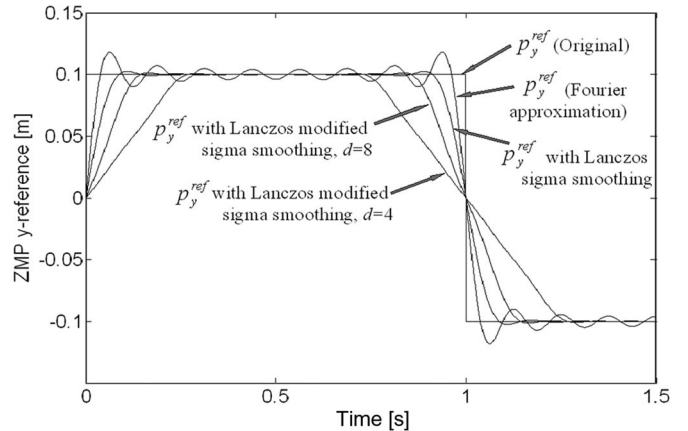

Fig. 12. Introduction of a double support phase by the modified Lanczos sigma smoothing with factors in (28). The parameter d can be chosen for desired double support phase duration. Longest double support period is observed with $d = 4$ in the figure.

The action of this smoothing mechanism is weighting the Fourier coefficients, and the higher the frequencies, the lower are the weighting gains (Fig. 10).

Fig. 11 shows the effects of the Lanczos sigma factors on the x- and y-direction ZMP references. The corresponding CoM references (c_x^{ref} and $c_y^{\text{ref}}(t)$) can be found by weighting the Fourier coefficients β_k and b_k in (19) and (24), respectively, by the same corresponding Lanczos sigma factors. The double
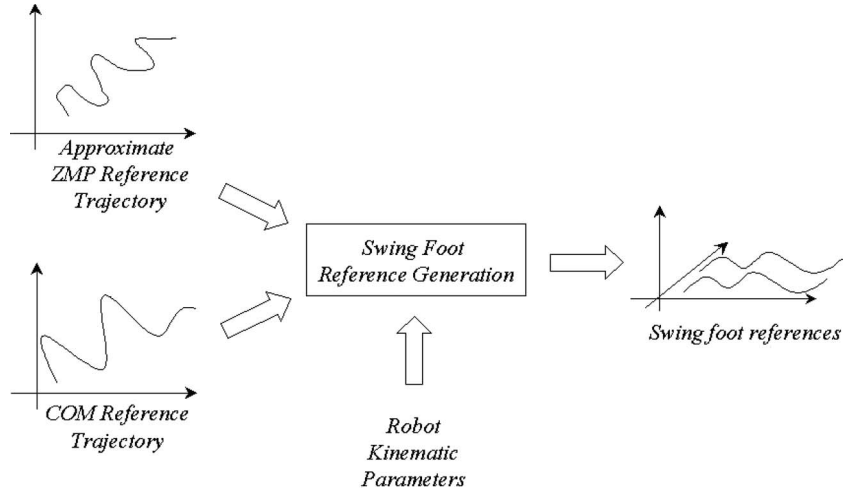
Fig. 13.   Swing foot references are obtained from ZMP and CoM references.
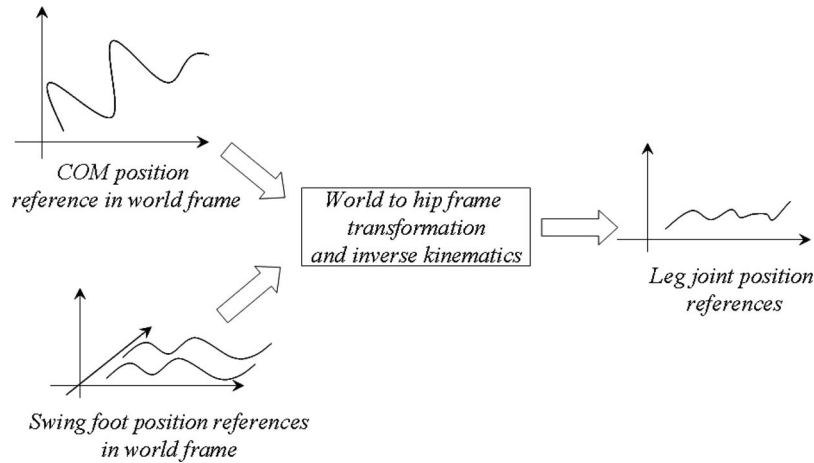

Fig. 14.   Leg joint position references are obtained via inverse kinematics.

support phase duration can be adjusted by an extension of the Lanczos Sigma smoothing algorithm. This is carried out by virtue of a double support phase parameter d. This parameter is used in place of N (the number of summed terms $+1$) in the Lanczos sigma factors in the sinc function

$$\text{sinc}(k\pi/d). \tag{28}$$

The effect of this modified Lanczos sigma smoothing is shown in Fig. 12 for the $p_y^{\text{ref}}(t)$. The parameter d can be chosen for desired double support phase duration. Longest double support period is observed with $d = 4$ in the figure.

This concludes the CoM reference generation section. The next section outlines the swing foot reference generation and locomotion control.

III. OUTLINE OF THE CONTROL ALGORITHM

The swing foot position references are obtained from ZMP and CoM references (Fig. 13). The control algorithm is a simple one based on independent joint PID position controllers. The joint position references are generated through inverse kinematics from CoM and swing foot references defined in world frame coordinates (Fig. 14). The foot orientation references used in

TABLE I
MASSES AND DIMENSIONS OF THE ROBOT LINKS

Link	Dimensions (LxWxH) [m]					Mass [kg]
Trunk	0.2	x	0.4	x	0.5	50
Thigh	0.27	x	0.1	x	0.1	12
Calf	0.22	x	0.05	x	0.1	0.5
Foot	0.25	x	0.12	x	0.1	5.5

inverse kinematics are fixed, and they are computed for feet parallel to the robot body. The PID controller gains are obtained via trial and error. The controller structured this way, except for the joint PID controllers, is an open-loop one. However, it achieves walking when stable reference trajectories (like the ones obtained in the previous section) are employed.

IV. SIMULATION RESULTS

The biped model used in this paper consists of two 6-DOF legs and a trunk connecting them (Fig. 1). Three joint axes are positioned at the hip. Two joints are at the ankle and one at the knee. Link sizes and the masses of the biped are given in Table I.
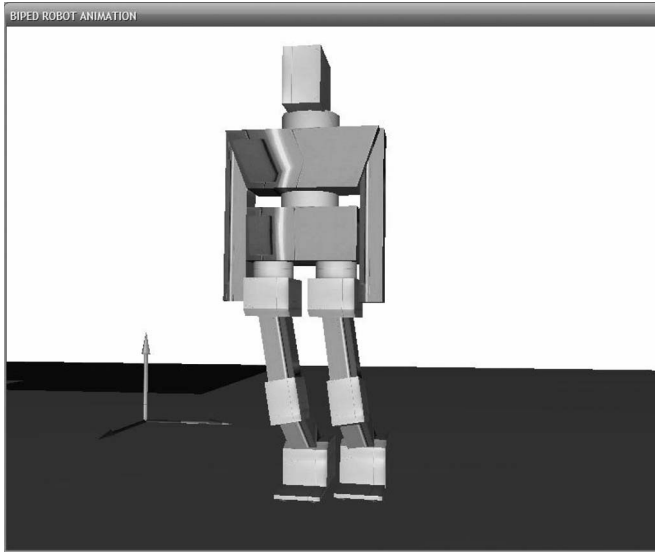
Fig. 15.   Snapshot from biped robot animation.

TABLE II
SOME OF THE IMPORTANT SIMULATION PARAMETERS

Parameter	Value
Step height	0.02 m
Step period	3 s
Foot to foot y-direction distance	0.16 m
Foot to foot y-direction ZMP reference distance	0.2 m
Step size	0.2 m
ZMP motion under the support foot	0.08 m

Simulations studies are carried out with this robot model, references generated in Section II and the coordination and control mechanism discussed in Section III. A view of the animation window is shown in Fig. 15. The full-dynamics 3-D simulation scheme is similar to the one in [30]. The ground contact is modeled by an adaptive penalty-based method. The details of the simulation algorithm and contact modeling can be found in [31]. Parameters used for reference generation are presented in Table II.

Fig. 16 shows the CoM position and CoM reference position projection on the ground plane for a 11 step walk. It can be observed that the COM reference is only roughly tracked. In the single support phases, the deviation from the reference curve is more pronounced. This suggests that the simple LIMP model, concentrating on the robot trunk, and ignoring the effects of the swing foot on the CoM of the whole robot, may encounter problems when the leg weight is not very low. The legs weigh 15 kg. Although it is much less than the 50-kg trunk weight, this weight significantly affects the CoM curve.

Although there are some tracking problems as discussed above, the reference generation and control algorithms are generally successful in keeping a stable walk and enabling the robot move forward with an almost constant speed of 7 cm/s. This is achieved without the need for the elaborate trial and error steps common to many other reference generation approaches.

For comparison purposes, simulations with fixed support foot ZMP references are also carried out. Exactly the same
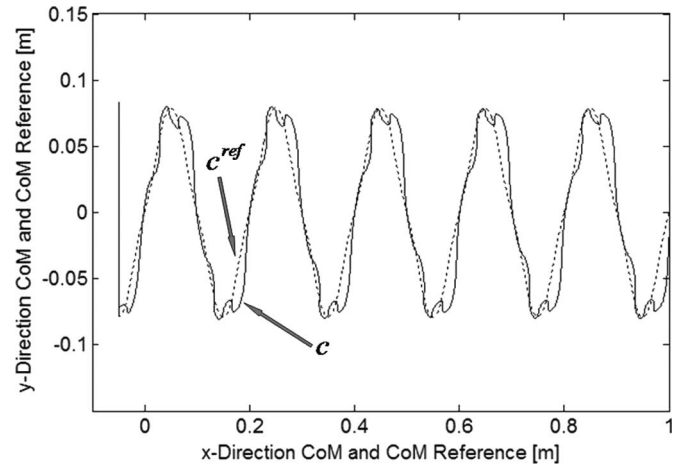

Fig. 16.   CoM position and CoM reference position projections on the $x-y$ plane (ground plane) with moving support foot ZMP references.
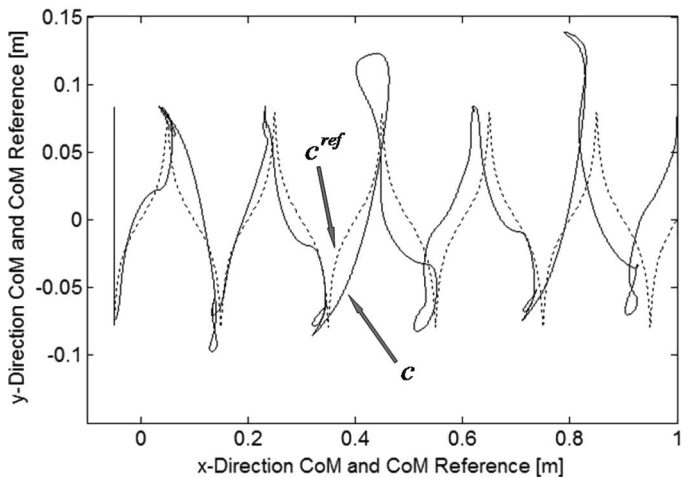

Fig. 17.   CoM position and CoM reference position projections on the $x-y$-plane with fixed support foot ZMP references.

independent joint position control scheme is applied without modifications. The CoM position and CoM reference position projections on the ground plane are shown in Fig. 17 for the fixed ZMP reference case. Again, a steady walk is obtained. However, the CoM trajectory deviates more from its reference with this kind of reference generation. Our observation from the animations is that in the simulations with fixed ZMP references, the robot body inclines with larger angles at every step when compared with the moving ZMP reference case. This is mainly due to higher cyclic acceleration and deceleration demands of the CoM reference (Fig. 9) obtained from the fixed ZMP reference curve. This result is in parallel with the findings in [21] and [22] supports the view that a more natural walk can be achieved with mowing support foot ZMP references.

As mentioned in Section I, the energy efficiency can be a measure of the naturalness of the walk too. The two cases, with the moving and fixed support foot ZMP references are compared in face of energy efficiency too. For this purpose, the energy consumed in one walk cycle (from one landing instant of the right foot to the next landing instant of the same foot)

TABLE III
ENERGY REQUIREMENTS FOR ONE WALK CYCLE

Reference generation algorithm	E_1	E_2
Moving support foot ZMP	45 J	147 J
Fixed support foot ZMP	70 J	201 J

is computed. This computation can be carried out by different ways. In one approach, as in [34] the integral

$$E_1 = \int_{t_1}^{t_2} \dot{\theta}^{\mathrm{T}} \tau dt \qquad (29)$$

where E_1 is the energy consumed in one walk cycle by the robot and t_1 and t_2 are the beginning and end times of the walk cycle, respectively. $\dot{\theta}$ and τ are joint velocity and joint torque vectors, respectively, as defined for (1). Equation (29) assumes that regenerative feedback to the supply is possible. In the nongenerative case where the braking energy is dissipated as heat the expression

$$E_2 = \int_{t_1}^{t_2} |\dot{\theta}^{\mathrm{T}} \tau| dt \qquad (30)$$

where $|\cdot|$ represents the absolute value function can be used in the computation of the energy requirement for one walk cycle. The $\dot{\theta}$ and τ histories recorded during simulation can be used to compute the expressions in (29) and (30). The results are tabulated in Table III, and they indicate that the moving ZMP reference considered in this section is 25%–30% more efficient than the fixed ZMP reference.

This result also supports the view that moving support foot ZMP curves are more natural than the fixed ones. It is also intuitive to think that a straight line, in place of the curved CoM references in Fig. 9 would the best choice for energy efficiency. Unnecessary cyclic acceleration and deceleration, which consume energy, would be avoided by a linear CoM x-direction reference. Note that a linearly increasing x-component would mean zero CoM acceleration in the x-direction and, by (4), the ZMP and CoM curves would coincide in the x-direction. Hence, a linearly increasing CoM x-component corresponds to a linearly increasing ZMP x-component. This would imply the same and constant ZMP x-direction velocity in the single and double support periods. Fig. 6(b) suggests that this can be achieved by a proper selection of the parameter $b(b = B/2)$. This, however, is where the two ways of defining the naturalness of the walk (the naturalness of ZMP trajectory and the energy efficiency) do not agree, as the experimental results in [21] and [22] indicate that human ZMP travels faster in the double support phase than in the single support phase.

V. CONCLUSION AND FUTURE DIRECTIONS

A trajectory generation, coordination and control approach for biped walking robots is presented in this paper. Humanlike ZMP reference trajectories with Fourier series approximation techniques for the solution of LIPM dynamics equations are employed in order to achieve naturalness in the walk. A simple

independent joint position controller structure is employed. Simulation studies show that the reference generation without considering the effects of the swing foot on robot ZMP can lead to significant deviations from reference trajectories. The walk, however, is stable and this is promising result making the algorithm a candidate for implementation. Swing foot motion compensation techniques and methods for the soft landing can be applied as future work in order to improve the controller performance. As an additional result, the comparison of the moving and fixed support foot ZMP references indicate that better energy efficiency can be obtained with moving references.

REFERENCES

[1] Y. Sakagami, R. Watanabe, C. Aoyama, M. Shinichi, N. Higaki, and K. Fujimura, "The intelligent ASIMO: System overview and integration," in *Proc. IEEE Int. Conf. Intell. Robots Syst.*, Lausanne, Switzerland, Oct. 2002, pp. 2478–2483.

[2] T. Sawada, T. Takagi, and M. Fujita, "Behavior selection and motion modulation in emotionally grounded architecture for QRIO SDR-4XII," in *Proc. IEEE Int. Conf. Intell. Robots Syst.*, Sendal, Japan, Oct. 2004, vol. 3, pp. 2514–2519.

[3] K. Loffler, M. Gienger, F. Pfeiffer, and H. Ulbrich, "Sensors and control concept of a biped robot," *IEEE Trans. Ind. Electron.*, vol. 51, no. 5, pp. 972–980, Oct. 2004.

[4] S. Lohmeier, K. Löffler, M. Gienger, H. Ulbrich, and F. Pfeiffer, "Computer system and control of biped 'Johnnie'," in *Proc. IEEE Int. Conf. Robot. Autom.*, New Orleans, LA, Apr. 2004, vol. 4, pp. 4222–4227.

[5] K. Kaneko, F. Kanehiro, S. Kajita, K. Yokoyama, K. Akachi, T. Kawasaki, S. Ota, and T. Isozumi, "Design of prototype humanoid robotics platform for HRP," in *Proc. IEEE Int. Conf. Intell. Robots Syst.*, Oct. 2002, vol. 3, pp. 2431–2436.

[6] Y. Ogura, H. Aikawa, K. Shimomura, H. Kondo, A. Morishima, H. Lim, and A. Takanishi, "Development of a humanoid robot WABIAN-2," in *Proc. IEEE Int. Conf. Robot. Autom.*, May 2006, pp. 76–81.

[7] K. Hirai, M. Hirose, Y. Haikawa, and T. Takenaka, "The development of Honda humanoid robot," in *Proc. IEEE Int. Conf. Robot. Autom.*, May 1998, vol. 2, pp. 1321–1326.

[8] M. Vukobratovic, B. Borovac, D. Surla, and D. Stokic, *Biped Locomotion: Dynamics, Stability and Application*. Berlin, Germany: Springer-Verlag, 1990.

[9] M. Raibert, *Legged Robots that Balance*. Cambridge, MA: MIT Press, 1986.

[10] S. Kajita and K. Tani, "Study of dynamic biped locomotion on rugged terrain—Theory and basic experiment-," in *Proc. 5th ICAR*, Jun. 1991, vol. 1, pp. 741–746.

[11] S. Kajita, K. Kaehiro, K. Kaneko, K. Fujiwara, K. Yokoi, and H. Hirukawa, "A real time pattern generator for bipedal walking," in *Proc. IEEE Int. Conf. Robot. Autom.*, May 2002, vol. 1, pp. 31–37.

[12] S. Kajita, F. Kanehiro, K. Kaneko, K. Yokoi, and H. Hirukawa, "The 3D linear inverted pendulum mode: A simple modeling for a biped walking pattern generation," in *Proc. IEEE/RSJ Int. Conf. Intell. Robots Syst.*, Oct. 29–Nov. 3 2001, vol. 1, pp. 239–246.

[13] S. Kajita, F. Kahehiro, K. Kaneko, K. Fujiwara, K. Harada, K. Yokoi, and H. Hirukawa, "Biped walking pattern generation using preview control of the zero-moment-point," in *Proc. IEEE Int. Conf. Robot. Autom.*, Taipei, Taiwan, Sep. 2003, vol. 2, pp. 1620–1626.

[14] T. Sugihara, Y. Nakamura, and H. Inoue, "Real-time humanoid motion generation through ZMP manipulation based on inverted pendulum control," in *Proc. IEEE Int. Conf. Robot. Autom.*, Washington, DC, May 2002, vol. 2, pp. 1404–1409.

[15] K. K. Noh, J. G. Kim, and U. Y. Huh, "Stability experiment of a biped walking robot with inverted pendulum," in *Proc. 30th Annu. Conf. IEEE IECON*, Nov. 2–6, 2004, vol. 3, pp. 2475–2479.

[16] M. Shibuya, T. Suzuki, and K. Ohnishi, "Trajectory planning of biped robot using linear pendulum mode for double support phase," in *Proc. 32nd Annu. Conf. IEEE IECON*, Nov. 2006, pp. 4094–4099.

[17] K. Harada, S. Kajita, K. Kaneko, and H. Hirukawa, "Dynamics and balance of a humanoid robot during manipulation tasks," *IEEE Trans. Robot.*, vol. 22, no. 3, pp. 568–575, Jun. 2006.

[18] E. Neo, K. Yokoi, S. Kajita, and K. Tanie, "Whole-body motion generation integrating operator's intention and robot's autonomy in controlling

humanoid robots," *IEEE Trans. Robot.*, vol. 23, no. 4, pp. 763–775, Aug. 2007.

[19] S. Kajita, T. Nagasaki, K. Kaneko, and H. Hirukawa, "ZMP-based biped running control," *IEEE Robot. Autom. Mag.*, vol. 14, no. 2, pp. 63–72, Jun. 2007.

[20] K. Harada, S. Kajita, F. Kanehiro, K. Fujiwara, K. Kaneko, K. Yokoi, and H. Hirukawa, "Real-time planning of humanoid robot's gait for force-controlled manipulation," *IEEE/ASME Trans. Mechatronics*, vol. 12, no. 1, pp. 53–62, Feb. 2007.

[21] A. Dasgupta and Y. Nakamura, "Making feasible walking motion of humanoid robots from human motion capture data," in *Proc. IEEE Int. Conf. Robot. Autom.*, Detroit, MI, May 1999, pp. 1044–1049.

[22] K. Erbatur, A. Okazaki, K. Obiya, T. Takahashi, and A. Kawamura, "A study on the zero moment point measurement for biped walking robots," in *Proc. 7th Int. Workshop Adv. Motion Control*, Maribor, Slovenia, 2002, pp. 431–436.

[23] C. Zhu, Y. Tomizawa, X. Luo, and A. Kawamura, "Biped walking with variable ZMP, frictional constraint, and inverted pendulum model," in *Proc. IEEE Int. Conf. Robot. Biomimetics*, Shenyang, China, Aug. 2004, pp. 425–430.

[24] O. Kurt and K. Erbatur, "Biped robot reference generation with natural ZMP trajectories," in *Proc. 9th IEEE Int. Workshop AMC*, Istanbul, Turkey, 2006, pp. 403–410.

[25] J. T. Todd, "Perception of gait," *J. Exp. Psychol. Hum. Percept. Perform.*, vol. 91, no. 1, pp. 31–42, Feb. 1983.

[26] J. E. Boyd and J. J. Little, "Phase in model-free perception of a gait," in *Proc. Workshop Human Motion*, Jul. 2000, pp. 3–10.

[27] J. Rose and J. G. Grimble, *Human Walking*. Baltimore, MD: Williams & Wilkins, 1994.

[28] Y. Choi, B. J. You, and S. R. Oh, "On the stability of indirect ZMP controller for biped robot systems," in *Proc. Int. Conf. Intell. Robots Syst.*, Sendal, Japan, Jun. 2004, vol. 2, pp. 1966–1971.

[29] O. Ayhan and K. Erbatur, "Biped robot walk control via gravity compensation techniques," in *Proc. 32nd Annu. Conf. IEEE IECON*, Nov. 6–10, 2005, pp. 1797–1802.

[30] Y. Fujimoto and A. Kawamura, "Simulation of an autonomous biped walking robot including environmental force interaction," *IEEE Robot. Autom. Mag.*, vol. 5, no. 2, pp. 33–42, Jun. 1998.

[31] K. Erbatur and A. Kawamura, "A new penalty based contact modeling and dynamics simulation method as applied to biped walking robots," in *Proc. FIRA World Congr.*, Vienna, Austria, Oct. 1–3, 2003. [CD-ROM].

[32] R. W. Hamming, "Lanczos' σ factors and 'The σ factors in the general case.' §32.6 and 32.7," in *Numerical Methods for Scientists and Engineers*, 2nd ed. New York: Dover, 1986, pp. 534–536.

[33] J. Foster and F. B. Richards, "The Gibbs phenomenon for piecewise-linear approximation," *Amer. Math. Monthly*, vol. 98, pp. 47–49, 1991.

[34] Y. Fujimoto, "Minimum energy biped running gait and development of energy regeneration leg," in *Proc. 8th IEEE Int. Workshop Adv. Motion Control*, Mar. 2004, pp. 415–420.

Kemalettin Erbatur (M'01) received double major B.S. degrees (with honors) in electronic engineering and mathematics from Bogaziçi University, Istanbul, Turkey, in 1992, the M.Sc. degree in control systems from Imperial College, London, U.K., in 1993, and the Ph.D. degree in electronics engineering from Bogaziçi University in 2000.

In 1993, he was with the Robotics and Automation Group, TUBITAK Marmara Research Centre, Gebze-Kocaeli, Turkey. In 1997, he became the leader of this group. After his Ph.D. studies, between 2000 and 2002, he had a Visiting Researcher position with The New Industry Research Organization, Kobe, Japan, followed by a Visiting Faculty position with the Electrical and Computer Engineering Department, Yokohama National University, Yokohama, Japan. Since 2002, he has been with the Faculty of Engineering and Natural Sciences, Sabanci University, Istanbul, Turkey, where he is currently a faculty member. For a period in 2003, he was a Collaborator of the International Rescue System Institute, Kobe, Japan, as a faculty of Sabanci University. He teaches courses on robotics, automation, and control. His primary research interests include intelligent motion control and humanoid robots. He is the author of more than 60 papers which have appeared in conference proceedings and journals.

Okan Kurt received the B.S. degree (with honors) in mechanical engineering from Yildiz Technical University, Istanbul, Turkey, in 2004, and the M.Sc. degree in mechatronic engineering from Sabanci University, Istanbul, Turkey, in 2006.

Currently, he is with the Product Development Department, Ford Otosan A. Ş., Kocaeli, Turkey. His research interests include mobile robotics and vibration engineering.